Table 1. Caisson Properties

Property	Model	Prototype
Outside Diameter	4.96 cm	3.47 m
Effective Length	10.16 cm	7.52 m
Total Length	11.43 cm	8.46 m
Shell Thickness	0.61 mm	45.14 cm
Vent Diameter	6.35 mm	47.00 cm
Young's Modulus	69.00 GPa	69.00 GPa

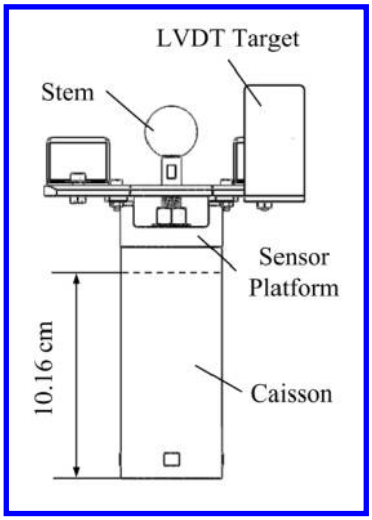

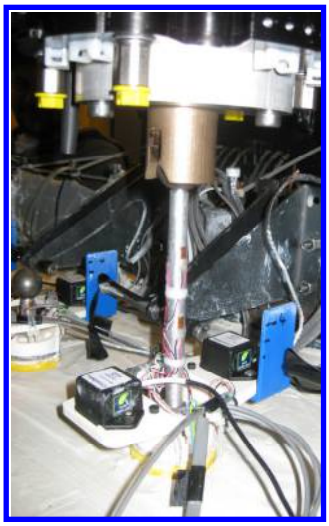

FIG. 2a. Monopile sketch (not to scale) **FIG. 2b. Example monopile loading**

The sensors platform was printed in multiple parts from ABS plastic on a 3D printer and fastened together with screws. The platform provided mounting space for two MEMS accelerometers and a target for the LVDT transducer, Figure 2a-b. The MEMS accelerometers had a ±10 g range (MEMSIC n.d.) and allowed for measurements of monopile rotation relative to centrifuge gravity.

Model Layout

The model presented below is the same as Experiment Two in Grajales et al. (2015). This paper addresses cyclic behavior of monopiles while Grajales et al. (2015) presented post-cyclic capacity.

After excavation of the soil bed the monopiles were installed by hand in 1 g. Three monopiles were installed on the center line of the box 18.5 cm on center with a foam template, Figure 3. The monopiles were installed until the plug was filled, a depth of 10.16 cm (assuming no plug heave). The vent was then plugged with a cork. LVDT transducers were mounted to the Large Rigid Box to measure pile translation. The LVDT sensors did not work well and are not presented. Displacement data instead comes from the theoretical motion of robot bounded by the MEMS accelerometer data (Beemer 2016). Pore pressure sensors were embedded in the soil during the bed

construction. The sensors were installed at monopile mid-depth, approximately 5 cm, and 3.81 cm away in the +X direction from the monopile. A mudmat 3D printed in ABS plastic was installed at the far end of the box. It carried a 100g MEMS accelerometer (Silicone Design Inc. 2013) at the height of the sensors platform on the monopiles. This was used to increase the accuracy of orientation measurements from the MEMS accelerometers on the monopiles (Beemer et al. 2015).

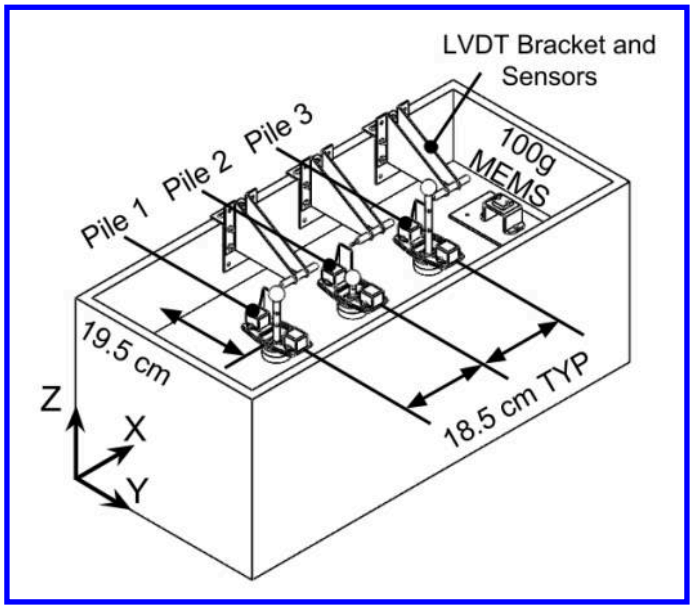

FIG. 3. Sketch of experimental layout

Finally, the model was center on the centrifuge basket such that the three monopiles and mudmat were aligned in the plane of Earth's gravity and centrifugal acceleration and the X-Z plane (Figure 3) was parallel to it.

TEST METHODOLOGY

The nominal centrifuge gravity for the experiment was 70 g; however, gravity at the caisson mid-depth was computed to be 74 g from the 100 g MEMS accelerometer. This acceleration has been used for all prototype scaling. In this experiment displacement magnitude and eccentricity were varied across the three monopiles. Additionally, each pile had a different vertical load due to self-weight from the caisson cap, stem, and sensor platform, Table 2. Monopile vertical capacity was estimated as 225 Newtons. Approximately 60%-78% of vertical capacity was engaged. Each foundation was loaded under three sets of 50 cycle one-way displacement controlled loading. A complete testing matrix for the cyclic loading portion of the experiment is provided in Table 2.

To ensure a constant strain rate over the duration of the one-way motion the maximum horizontal velocity could only be 2 mm/s. This is because the RPI 4 DOF robot's maximum acceleration is 50 mm/s^2. This combination of acceleration velocity ensured that at least 95% of each motion was at a constant strain rate and the caisson's behavior was undrained. The normalized velocity, $V = vd/c_v$, eccentricity

was of 625; well above the minimum for undrained conditions of 30 (DeJong et al., 2012). Displacement magnitudes in Table 2 are at eccentricity, they were selected to bound working and failure limit states at the soil surface.

Table 2. Experiment Cyclic Loading Matrix

Monopile (#)	Load Eccentricity (Ø)	Model Vertical Load (N)	Test (#)	Displacement Magnitude (% Ø)	One-Way Load Direction ±(X,Y,Z)	Cycles (#)
1	2.27	175.0	1	2.5	+X	50
			2	5.0	+X	50
			3	10	+X	50
2	1.10	135.0	1	2.5	+X	50
			2	5.0	+X	50
			3	10	+X	50
3	3.05	150.0	1	2.5	+X	50
			2	5.0	+X	50
			3	10	+X	50
where: Ø = caisson diameter, 4.96 cm						

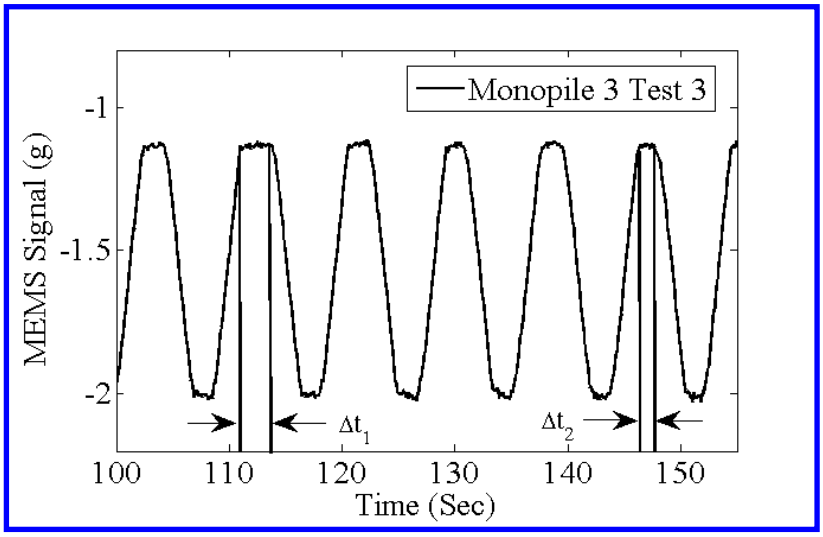

FIG. 4. Example of variation in robot motion due to anti-collision algorithm

Also of note, is that prior to making any motion the RPI 4 DOF Robot runs an anti-collision algorithm. The computation time to complete these calculations varied significantly as seen in MEMS accelerometer signal in Figure 4, $\Delta t_1 > \Delta t_2$. Thus the load frequency and period were not constant. Target load periods (calculated from robot acceleration, velocity, and displacement magnitude) and applied load periods (total cycling time divided by number of cycles) have been provided in Table 3. On average the pauses by the robot added 3.70 seconds to the load period, at model scale. The only foreseeable impact this would have on results is if setup occurred during the

pauses. The average pause time at prototype scale was 2.8 hours. This should not have been enough time for any significant setup to occur.

As discussed in the **Results** section significant settlement of the monopiles occurred during cycling. There was concern that if too much settlement occurred the stem and robot would decouple. To prevent this a small vertical motion of 1.5% of diameter (0.75 mm) was added to the robot cyclic program after 25 cycles.

Table 3. Target vs applied load period

Monopile (#)	Test (#)	Displacement Magnitude (% Ø)	Target Load Period (s)	Applied Load Period (s)	Prototype Applied Period (min)
1	1	2.5	1.64	5.48	6.76
	2	5.0	2.88	6.56	8.09
	3	10	5.38	8.81	10.87
2	1	2.5	1.64	5.65	6.97
	2	5.0	2.88	6.54	8.07
	3	10	5.38	9.02	11.12
3	1	2.5	1.64	5.52	6.81
	2	5.0	2.88	6.53	8.05
	3	10	5.38	8.85	10.92

RESULTS

Initial Orientation of Piles

During centrifuge spin up all three monopiles tilted slightly in the –X direction. There was concern that these initial movements of the monopiles would result in the LVDT sensors going out of range during testing; so, Monopiles 1 and 3 were straighten to ensure this would not occur. Both piles were allowed to sit for 5 minutes, 19 days in prototype time at 74 g, to allow any generated excess pore pressures to dissipate. Adjusted locations and initial monopile tilts from MEMS accelerometers, after adjustment, are provided in Table 4. It should be noted initial tilt of the pile is difficult to ascertain because the basket orientation relative to centrifuge gravity was not measured during the experiment. The largest sources of uncertainty in orientation of the basket comes from the robot changing the model's center of gravity and applied moment about the basket hinge, see Beemer at al. (2016). However, given that the model was centered in the basket and the RPI robot was center when over Monopile 2 it is likely error in initial tilt is on the order of ±1°-3°.

Pile Settlement

As noted previously significant settlement occurred during cycling. The RPI robot was used to measure settlement. After each test the robot was stepped in 0.1 mm increments until it fully connected with the stem. The measurement was taken as change in robot vertical coordinate. Settlement appears to be dependent on load

eccentricity, Table 5, and is not due to consolidation. As seen in Table 2 Monopile 1 had the largest gravity load, but it settled less than Monopile 3 which had a much lighter load. Additionally, the model sat for 7 months of prototype time at 74 g (excluding centrifuge spin up); enough time for the majority primary consolidation to be completed, before testing. It is possible that the combined lateral-vertical load results in plastic failure; given the high ratio of vertical to horizontal load any plastic deformation would include a significant vertical movement.

Table 4. Initial Pile Orientation

Monopile (#)	Pre-Spin Up Robot X-Location (mm)	Post-Spin Up Robot X-Location (mm)	Adjusted Robot X-Location (mm)	Adjusted Tilt MEMS (°)
1	227	213.0	227	4.63
2	417	412.0	413	1.20
3	598	579.5	585	2.15

Table 5. Monopile Settlement

Test (#)	Monopile 1	Monopile 2	Monopile 3
	Eccentricity = 2.25 Ø	Eccentricity = 1.10 Ø	Eccentricity = 3.05 Ø
	Prototype Settlement (cm)		
1	29.6	22.20	37.0
2	22.2	14.80	22.2
3	22.2	22.20	22.2
Total:	74.0	59.20	81.4
Total (d/L):	9.80 %	7.90 %	10.80 %

Effects of Load Eccentricity and Depth of Rotation

The following section discusses the impact of varying load eccentricity on monopile cyclic behavior. A sketch of monopile reaction has been provided in Figure 5 for reference. Monopile 1 with an eccentricity of 2.25 had the largest resistance to rotation across all displacement magnitudes at eccentricity, example in Figure 6. This is in spite of the fact that Monopile 2 rotated and displaced more than Monopile 1, Figure 7a-b. Reactive moment appears to be dependent on depth of rotation and not load eccentricity, Figure 8a-b. Maximum rotational resistance appears to correspond with the shallowest depth of rotation. Though Monopile 2 rotated more than Monopile 1 its deep depth of rotation indicates its behavior was more translational than rotational resulting in decreased moment resistance. It is also interesting that Monopile 3 had a deeper depth of rotation than Monopile 1. This indicates that small differences in initial orientation of the monopile could have a large impact on rotational resistance. Monopile 1 had an initial tilt of 4.63° while Monopile 3 had an initial tilt of only 2.15°. The initial tilt may reduced the depth of rotation.

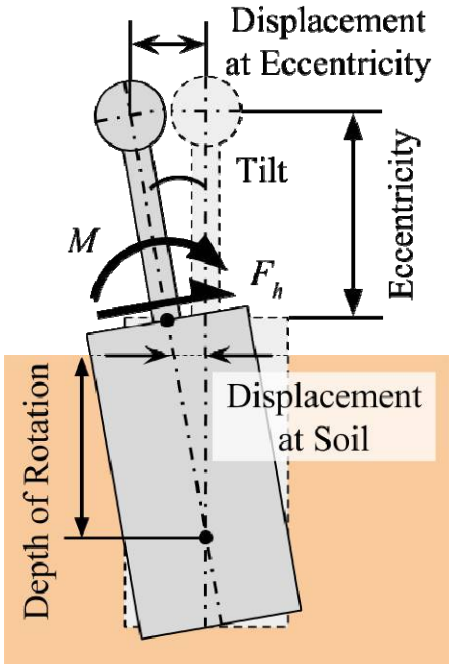

FIG. 5. Monopile Loading and Reactions

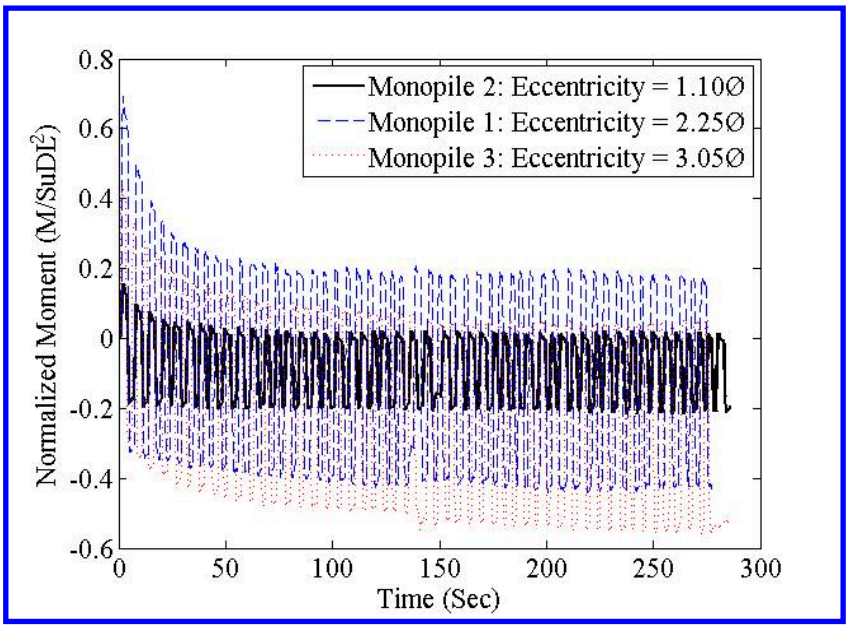

FIG. 6. Reactive Moment All Monopiles, Test 2, Displacement 2.5% Ø

Monopile tilt appears to stabilize quickly and remains constant after a few cycles, Figures 7a. It also appears to increase incrementally for both a decrease of load eccentricity and an increase in displacement magnitude. Though load, moment, and tilt behaviors are fairly stable, displacement at the soil surface appears to drift; with Monopile 1 and 3 drifting in opposite directions, Figures 7b.

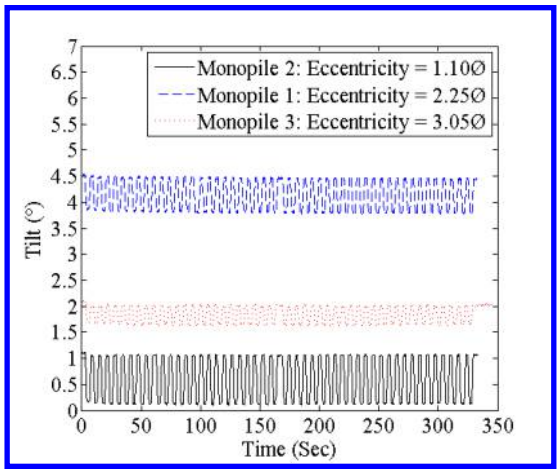

FIG. 7a. Tilt All Monopiles, Test 2, Displacement = 2.5% Ø

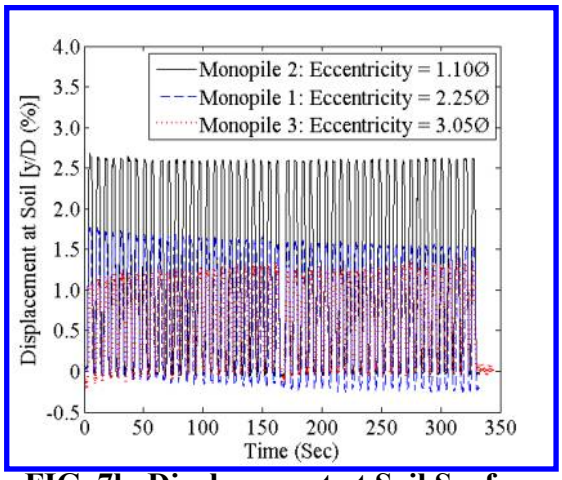

FIG. 7b. Displacement at Soil Surface All Monopiles, Test 2, Displacement = 2.5% Ø

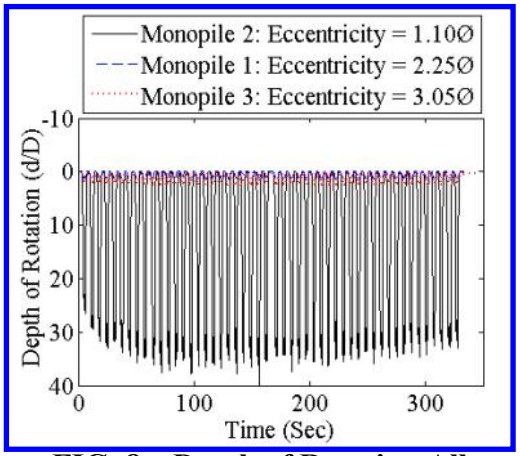

FIG. 8a. Depth of Rotation All Monopiles, Test 2, Displacement 2.5% Ø

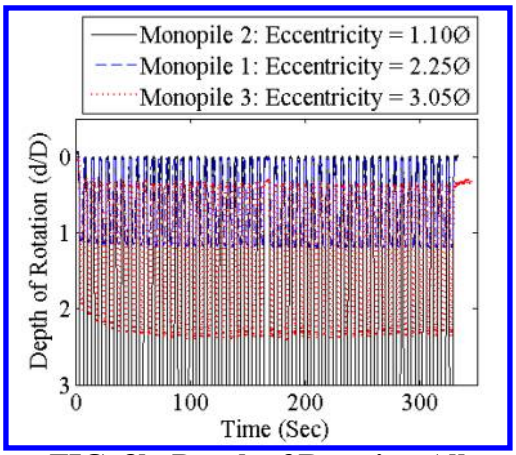

FIG. 8b. Depth of Rotation All Monopiles, Test 2, Displacement 2.5% Ø (Zoomed)

CONCLUSIONS

The initial results from these geotechnical centrifuge experiments provide some insights into the rotational behavior of squat monopiles in soft clay:

1. Monopiles with vertical gravity loads settle significantly under cyclic loading. This may be the result of combined vertical-horizontal-moment loading causing vertical plastic deformation
2. Moment resistance appears dependent on depth of rotation not, specifically, load eccentricity. Initial tilt could have a large impact on depth of rotation and therefore rotational resistance. The pile with the shallowest depth of rotation and highest resistance, had the most initial tilt and not the largest eccentricity.
3. Monopile tilt stabilizes quickly under displacement controlled loading
4. Monopiles appear to translate horizontally under displacement control loading

ACKNOWLEDGMENTS

The authors would like to acknowledge the assistance provided by the Center for Earthquake Engineering Simulations at Rensselaer Polytechnic Institute. This project was funded by National Science Foundation, Award Number: 1041604.

REFERENCES

Andersen, K. H., and Lauritzsen, R. (1988). "Bearing capacity for foundations with cyclic loads." J. of Geotech. Eng., ASCE, 114(5), 540–555.

Beemer, R. D. (2016). "Experimental studies of squat gravity caissons and piles for offshore applications." PhD Dissertation, Texas A&M University.

Beemer, R. D., Aubeny, C. P., and Biscontin, G. (2016). "Centrifuge model 2D gravity relative to the rotational reference frame." In Preparation.

Beemer, R. D., Murali, M., Biscontin, G., and Aubeny, C. P. (2015). "Theory on measuring orientation with MEMS accelerometers in a centrifuge." IFCEE, ASCE, San Antonio.

Dejong, J. T., Yafrate, N., Degroot, D. J., Low, H. E., and Randolph, M. F. (2012). "Recommended practice for full-flow penetrometer testing and analysis." Geotech. Test. J., ASTM International, 33(2), 1-13.

Elgamal, A., Dobry, R., and Van Laak, P. (1991). "Design, construction and operation of 100 g-ton centrifuge at RPI." Centrifuge 91, Boulder, CO, 27–34.

Garnier, J., Gaudin, C., Springman, S. M., Culligan, P. J., Goodings, D. J., Konig, D., Kutter, B. L., Phillips, R., Randolph, M. F., and Thorel, L. (2007). "Catalogue of scaling laws and similitude questions in geotechnical centrifuge modelling." Int. J. of Phys. Modell. in Geotech., ICE, 7(3), 1-23.

Grajales, F., Beemer, R. D., Murali, M., Aubeny, C. P., and Biscontin, G. (2015). "Response of short monopiles for offshore wind turbine foundations: virgin and post cyclic capacity." GeoQuebec, Canadian Geotechnical Society, Quebec City.

Lau, B. H. (2015). "Cyclic behaviour of monopile foundations for offshore wind farms." PhD Diss., University of Cambridge.

MEMSIC. (n.d.). CXL-GP series general purpose accelerometer. San Jose, CA.

Murali, M. (2015). "Characterization of soft clay and the response of soil-foundation system for offshore applications." PhD Diss., Texas A&M University.

Poulos, H. G., and Davis, E. H. (1991). *Elastic Solutions for Soil and Rock Mechanics*. Centre for Geotechnical Research, University of Sydney, Sydney.

Randolph, M. F. (1981). "The response of flexible piles to lateral loading." Geotechnique, ICE, 31(2), 247–259.

Silicon Design Inc. (2013). Model 2012. Kirkland, WA.

Tessari, A. (2012). "Centrifuge modeling of the effects of natural hazards on pile-founded concrete floodwalls." PhD Diss., Rensselaer Polytechnique Institute.

Ubilla, J., Abdoun, T., and Zimmie, T. (2006). "Application of in-flight robot in centrifuge modeling of laterally loaded stiff pile foundations." 6th ICPMG, Hong Kong, 259–264.

Zhang, C., White, D., and Randolph, M. F. (2011). "Centrifuge modeling of the cyclic lateral response of a rigid pile in soft clay." J. Geotech. and Geoenviron. Eng., ASCE, 137(7), 717–729.

Shear Behavior of Methane Hydrate Bearing Sands during Gas Production

Masayuki Hyodo[1]; Shintaro Kajiyama[2]; and Koji Nakashima[2]

[1]Professor, Dept. of Civil and Environmental Engineering, Ube 755-8611, Japan.
[2]Post Graduate Student, Dept. of Civil and Environmental Engineering, Ube 755-8611, Japan.

Abstract: A series of mechanical tests were performed on methane hydrate bearing sediments with various host sands by using temperature controlled high stress triaxial shear testing apparatus. A high pressure and low temperature plane strain testing apparatus was also developed for visualizing the deformation of methane hydrate bearing sand due to methane hydrate production. Using this testing apparatus, plane strain compression and methane hydrate dissociation by depressurization tests were performed with the measurement of localized deformation.

INTRODUCTION

Methane hydrate (MH) is a solid compound in which a large amount of methane is trapped within a crystalline structure of water, forming a solid similar to ice. Recently there has been much research into MH in the deep seabed as a developable material. Worldwide, MH is believed to exist in various forms, such as massive structures within muddy layers or at the surface of deep seabeds, or embedded within the pores of sandy layers (Waite, et al. 2009). In Japan, an MH rich layer was found in the Nankai Trough and production tests was performed in March 2013 (Japan Oil, Gas and Metals National Corporation, 2013). MH in the deep sea bed can exist at certain water pressure and temperature conditions. It exists in the pore space of the sandy sediments, bonding their particles. The MH rich layer is located around 100m-300m from the seabed, in deep seas with depths of over 1000m. Currently, the method proposed for abstracting methane in the Nankai Trough is by drilling a rig into the MH-rich layer, and heating, depressurising, or inserting hydrate inhibitors, causing the MH to become dissociated into methane and water after which the gas could be collected (Yamamoto, 2009). Among them the depressurisation method is going to be introduced as the most suitable production method. Using these methods, the solid MH existing in the pores within the soil is transformed into gas for collection; in the process, complex physical events, such as changes in the soil structure and thermal conductivity, pore fluid and gas migration, and other complicated phenomena need to be considered. It is predicted that a combination of such phenomena could cause consolidation and shear deformation of the ground due to changes in the effective stress and decrease in soil particle strength. Therefore, it is important to investigate the mechanical properties of MH-bearing

sediments, for safe and economical exploitation. A series of mechanical tests were performed on MH bearing sediments with various host sands by the authors using temperature controlled high stress triaxial shear testing apparatus. A high pressure and low temperature plane strain testing apparatus was also developed for visualizing the deformation of methane hydrate bearing sand due to methane hydrate production. Using this testing apparatus, plane strain compression and methane hydrate dissociation by depressurization tests were performed with the measurement of localized deformation.

MATERIALS USED IN EXPERIMENTS

Grain size distribution curves for samples from Nankai Trough and the simulation materials prepared in this study are shown in FIG.1. The sediments in Nankai Trough`s seabed soil constitute turbidite and show stratified layers with wide grain distribution curves, with contents ranging from sand to clay. The grain size distribution for the MH rich layer in Nankai Trough is shown in grey; it is mostly sand with fines content. In order to simulate the grain size distribution and minerals of this layer, silica sand, kaolin and mica were mixed and four kinds of simulated sands T_a, T_b, T_c, T_d were prepared as host sands. The fines content increases in order of T_b, T_a, T_c, T_d and the mean particle size decreases in order of T_a, T_b, T_c, T_d.

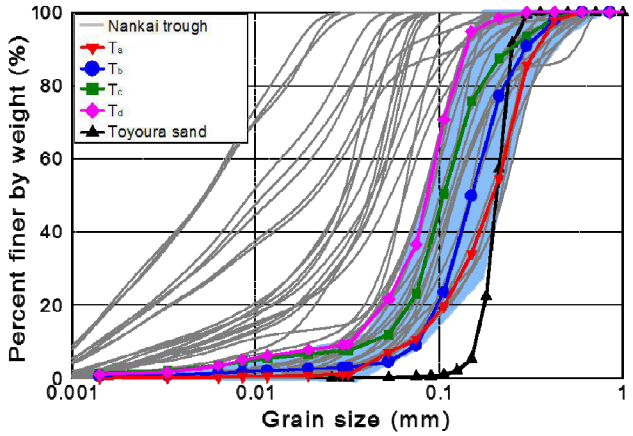

FIG.1. Grain size distribution curves (Nankai trough and artificial samples)

TEMPERATURE-CONTROLLED HIGH STRESS TRIAXIAL TESTS

The temperature-controlled high pressure triaxial testing apparatus was developed such that the back pressure and confining pressure could be controlled under various temperature and high pressure conditions in order to examine the mechanical behaviour of MH-bearing sand specimens under deep seabed stress and temperature conditions (Hyodo, et al., 2007, 2008, 2013). The maximum permissible load was 200kN. To remove the influence of piston friction, a cylindrical-shaped loading cell that was not affected by temperature and pressure was set up in the cell. The cell pressure could be increased up to 30MPa. To reproduce back pressure associated with this high pressure condition, a syringe pump was installed. By using incompressible solution in the cylinder, the measurement of volume change of the specimen was enabled by